On the Simulation of Composition Profiles in NiCoCrAl Alloys During Al2O3 Scale Growth in Oxidation and Oxidation-Dissolution Regimes

Thomas Gheno, Greta Lindwall

▶ **To cite this version:**

Thomas Gheno, Greta Lindwall. On the Simulation of Composition Profiles in NiCoCrAl Alloys During Al2O3 Scale Growth in Oxidation and Oxidation-Dissolution Regimes. Oxidation of Metals, 2018, pp.1-14. hal-01978273v1

HAL Id: hal-01978273

https://hal.science/hal-01978273v1

Submitted on 25 Jan 2019 (v1), last revised 19 Feb 2019 (v2)

HAL is a multi-disciplinary open access archive for the deposit and dissemination of scientific research documents, whether they are published or not. The documents may come from teaching and research institutions in France or abroad, or from public or private research centers.

L'archive ouverte pluridisciplinaire **HAL**, est destinée au dépôt et à la diffusion de documents scientifiques de niveau recherche, publiés ou non, émanant des établissements d'enseignement et de recherche français ou étrangers, des laboratoires publics ou privés.

On the simulation of composition profiles in NiCoCrAl alloys during Al_2O_3 scale growth in oxidation and oxidation-dissolution regimes

Thomas Gheno[1,*], Greta Lindwall[2]
[1]DMAS, ONERA, Université Paris Saclay, 92322 Châtillon, France
[2]Department of Materials Science and Engineering, KTH Royal Institute of Technology, 10044 Stockholm, Sweden

*Corresponding author. Email: thomas.gheno@onera.fr

Keywords: high temperature corrosion; molten silicate; interdiffusion; Calphad; thermodynamic database; mobility database

Abstract

The ability to simulate the oxidation behavior of multicomponent alloys is a powerful tool for alloy development and oxidation research. The present work shows how the DICTRA module of Thermo-Calc can be applied to reproduce composition profiles in NiCoCrAl alloys during Al_2O_3 scale growth when used in conjunction with appropriate Calphad thermodynamic and diffusion mobility databases. Profiles were calculated in pure oxidation and oxidation-dissolution regimes to simulate reaction in air and in a molten silicate. For each regime, a simple analytical expression was used to set the outward Al flux at the alloy surface as a boundary condition. The simulations were performed using different combinations of thermodynamic and diffusion mobility databases, which demonstrated the relative importance of the thermodynamic and kinetic contributions to the interdiffusion coefficients, and in turn to the concentration profiles. The simulations done with the developmental NISTCoNi-mob mobility database were found to be in good agreement with experimental data, while those done with MOBNI4 significantly underestimated Al depletion (and Co, Cr and Ni enrichment), due in part to an incomplete description of diffusivity in the Co-Ni binary system. The tested thermodynamic databases all yielded similar results. This work provides a quantitative illustration of the importance of critically assessed diffusion mobility descriptions in designing oxidation-resistant materials.

1 Introduction

High temperature alloys and coatings are designed to withstand aggressive environments via selective oxidation, a process whereby an alloying element preferentially reacts to form an adherent and slow-growing oxide scale, most often Cr_2O_3 or Al_2O_3. The selective removal of an element causes its depletion in the metal subsurface, and a sufficient flux of this element from the bulk to the surface is required for the external scale to remain stable. Furthermore, subscale composition variations may affect the materials microstructure, via precipitate dissolution for example, and in turn alter its properties. Oxidation-induced diffusion fluxes and composition variations should therefore be anticipated in designing materials and components.

Composition profiles associated with external scale growth can be calculated analytically from Wagner's theory [1] in the limiting case of a binary (or pseudo-binary), single-phase system with a constant interdiffusion coefficient. This model has been

extended in a number of ways (see for example Refs. [2-6]). However, applications of analytical methods remain limited, in part due to the difficulty of handling composition-dependent solubilities and diffusivities in multicomponent systems. The problem requires numerical resolution, which is typically done by a finite difference method.

Early finite difference models of oxidation-induced interdiffusion were reviewed in Ref. [7]. Whittle et al. [8] examined the effect of the oxidation rate law on depletion profiles in binary, single-phase alloys with a constant diffusion coefficient. Nesbitt [9,10] used composition-dependent interdiffusion coefficients adjusted on diffusion couple data to model oxidation in the ternary NiCrAl system, with a single-phase approximation. Lee et al. [11] introduced a simplified handling of two-phase equilibrium to simulate oxidation-induced β dissolution in γ-β CoCrAl coatings, but also approximated the two-phase region as a single-phase material to solve the diffusion equation.

Further progress in simulating interdiffusion in multicomponent, multiphase systems has been made possible by the use of the Calphad method [12,13] to describe composition-dependent thermodynamic and diffusion properties. In this method, the properties of each phase are described using standardized functions of the concentrations, with pure element properties and interaction parameters as coefficients. These parameters are organized in thermodynamic and diffusion mobility databases often dedicated to a given alloy system, e.g., Ni-based alloys, which have been the subject of important efforts. Interdiffusion is then addressed by coupling a minimization of the Gibbs energy, which provides equilibrium phase compositions and fractions, with a resolution of the diffusion equation, which yields fluxes and composition variations [14,15].

In early applications of the Calphad method to oxidation-induced interdiffusion, some authors implemented their own diffusion solver and mobility assessment, coupled with a thermodynamics software. More recently, simulations were also conducted using DICTRA, the diffusion solver integrated in the Thermo-Calc software package [16]. Examples of software and databases used in simulations of oxidation in Ni- and Co-based systems are given in Table 1.

Table 1: Thermodynamics and diffusion software and data used in multicomponent, multiphase oxidation-induced interdiffusion simulations in Ni- and Co-based systems reported in the literature. Refs: Thermo-Calc [16], TCNI [17], MOBNI [18], MTDATA [19], Ni-DATA [20](abbreviated as TTNI).

Reference	Thermodynamics		Diffusion	
	Solver	Database	Solver	Database
Nijdam 2008 [21]	Thermo-Calc	TTNI6	Own	Own assessment
Karunaratne 2009 [22]	MTDATA	TTNI*	Own	Own assessment
Bensch 2012 [23]	Thermo-Calc	TTNI7	DICTRA	MOBNI1
Yuan 2013 [25]	Thermo-Calc	TCNI5	DICTRA	MOBNI2
Pillai 2015 [24]	Thermo-Calc	TCNI5	Own	MOBNI2
Chen 2018 [26]	Thermo-Calc	TTNI7	DICTRA	MOBNI2

*version not specified

Nesbitt [7] noted in 1995 that access to appropriate diffusion data was key to the success of numerical simulations of interdiffusion during oxidation. Although much progress has been made since, especially in Ni-based systems, this remains relevant. The

present paper aims at illustrating the importance of diffusion data, using the example of NiCoCrAlY bondcoat compositions with relatively high Co and Cr levels. The kinetics of Al depletion during oxidation of model alloys in air and in molten sodium silicate were studied experimentally and via an approximate analytical model in Ref. [27]. In the concluding section of Ref. [27], it was noted that DICTRA simulations failed to predict accurate concentration profiles and that efforts were needed to better account for the effects of high Co levels in mobility databases. The present paper further examines this point using different thermodynamics and diffusion mobility databases.

2 Simulation methods and conditions

2.1 Diffusion models

The simulations were run in one-dimension using DICTRA version 2017a. For a description of how interdiffusion is handled in DICTRA, the reader is referred to Ref. [14]. Briefly, in an *n*-component system, the interdiffusion fluxes are defined in the volume-fixed frame of reference as:

$$\tilde{J}_k = -\sum_{j=1}^{n-1} \widetilde{D}_{kj}^{n} \frac{\partial C_j}{\partial z} \tag{1}$$

where the C_j are the component concentrations (mole per unit volume), z is the space coordinate in the diffusion direction, and the $\widetilde{D}_{kj}^{n}$ are the interdiffusion coefficients, where the n^{th} component has been chosen as the dependent component (here this component was Ni, but the choice was arbitrary and had no effect on the computed profiles). Only substitutional diffusion is considered here. The interdiffusion coefficients are defined as:

$$\widetilde{D}_{kj}^{n} = \sum_{i=1}^{n} (\delta_{ik} - x_k) x_i M_i \left(\frac{\partial \mu_i}{\partial x_j} - \frac{\partial \mu_i}{\partial x_n} \right) \tag{2}$$

where δ is the Kronecker delta ($\delta_{ik} = 1$ if $k = i$, 0 otherwise), and x_i, M_i and μ_i are the mole fraction, atomic mobility and chemical potential of component i, respectively. As seen in Eq. (2), the interdiffusion matrix comprises kinetic terms, in the form of the diagonal mobility matrix M, and thermodynamic terms (the $\frac{\partial \mu_i}{\partial x_j}$, i.e., the second-order partial derivatives of the Gibbs free energy), which allow for cross-component interactions. For a discussion of the hypotheses underlying Eq. (2), the reader is referred to Ref. [28].

The temperature dependence of the atomic mobility is typically described as:

$$M_k = \frac{M_k^0}{RT} \exp\left(-\frac{Q_k}{RT}\right) \tag{3}$$

The composition dependence of the pre-exponential factor M_k^0 and activation energy Q_k is described using a Redlich-Kister expansion:

$$\phi_k = \sum_{i=1}^{n} x_i \phi_k^i + \sum_{i=1}^{n} \sum_{j=i}^{n} x_i x_j \left[\sum_{r=0}^{m} {}^{r}\phi_k^{i,j} (x_i - x_j)^r \right] \tag{4}$$

where ϕ_k is $\ln(M_k^0)$ or Q_k, ϕ_k^i is the value of ϕ_k in pure i, ${}^{r}\phi_k^{i,j}$ are interaction parameters, and m is the order of the expansion. The ϕ_k^i and ${}^{r}\phi_k^{i,j}$ terms are together called mobility parameters and are the quantities stored in Calphad diffusion mobility

databases. In practice, mobility parameters are mostly determined from either interdiffusion data or tracer diffusion data; tracer diffusion coefficients D_k^* and atomic mobilities are related via:

$$D_k^* = RTM_k \tag{5}$$

The temperature and composition dependence of the chemical potentials are obtained from a Calphad thermodynamic database, which stores parameters for the Gibbs free energy of the phases, according to a formalism similar to that described above. For a thermodynamic database and a mobility database to be compatible, each phase should be described with the same sublattice model in both databases.

2.2 Databases and simulation conditions

The present work concerns NiCoCrAl alloys. Simulations were done using the commercial Ni-alloys databases TCNI8 [29] and MOBNI4 [30], and databases currently under development at the National Institute of Standards and Technology (NIST, USA) as part of the Center of Hierarchial Materials Design [31], referred to here as NISTCoNi and NISTCoNi-mob. These are extensions of the NIST Ni Superalloy thermodynamic [32] and mobility [33] databases previously developed for Ni-based systems, to account for Co-based systems as well as for systems with intermediate Co and Ni contents. These extensions are primarily motivated by the recent interest in Co-based superalloys [34], and also target the design of bondcoats rich in both Ni and Co. A thermodynamic database optimized for NiCoCrAl compositions, CRALDAD v1 [35,36], was also tested in the present work. The version of NISTCoNi-mob available to us at the time of the calculations did not contain the β-(Ni,Co)Al phase. Consequently, only experiments involving single-phase γ alloys were considered in the simulations. Given its small concentration in the alloys studied experimentally (0.1 at. %), Y was not included in the simulations.

The main settings of the simulations were:

- Planar geometry, linear grid (constant node spacing), 300 nodes, 900 μm long
- Initial condition: uniform concentrations (measured in alloys of nominal compositions (at. %) Ni-33Co-35Cr-7Al and Ni-28Co-19Cr-11Al [27])
- Backward Euler (implicit) resolution scheme

Although the simulations only involved single-phase alloys, use of the homogenization model [37] was enforced. This had no influence on the resolution per se, but changed the way boundary conditions were defined and allowed an easier implementation of the oxidation model. Considering the symmetry of the problem, the simulated material represented half-specimens. A zero-flux boundary condition was used on the bulk side (symmetry plane). To simulate the composition changes due to the growth of an external oxide scale, a corresponding flux of Al was set as a boundary condition on the surface side.

2.3 Oxidation model

Oxidation was modeled with the assumption that its rate is controlled by diffusion in the scale. At steady-state, the Al flux across the alloy/scale interface, $J_{\mathrm{Al}}^{\mathrm{out}}$, can then be expressed as:

$$J_{\mathrm{Al}}^{\mathrm{out}} = \frac{2}{V_{\mathrm{ox}}}\frac{k_p}{X} \tag{6}$$

where X is the scale thickness, V_{ox} the molar volume of the oxide, and k_p the parabolic constant. The scale was assumed to be pure Al_2O_3. (At 1100 °C, in the absence of a deposit, the alloys of interest form Al_2O_3 scales with small amounts of other oxides [38]. In molten sodium silicate, the alloys also form Al_2O_3, but Al-lean compositions such as Ni-33Co-35Cr-7Al are susceptible to local failure, where Al_2O_3 growth cannot be sustained and Cr_2O_3 forms instead [27]. The present simulations concern the Al_2O_3 growth stage).

In the absence of a molten silicate, the only contribution to scale growth is that of oxidation, Eq. (6). The time evolution of X is given by a mass balance on Al:

$$\frac{\mathrm{d}X}{\mathrm{d}t} = \frac{k_p}{X} \tag{7}$$

Integration of Eq. (7) with the initial condition $X(t=0) = X_0$ yields:

$$X^2 - X_0^2 = 2k_p t \tag{8}$$

It is recognized that oxidation kinetics are in general more complex than expressed by Eqs. (7-8), for a number of reasons. Nevertheless, once steady-state is reached, the approximation of parabolic kinetics is appropriate for the alloys and conditions of interest, as can be shown using the thermogravimetric data reported in Ref. [39] and other (unpublished) data from the same study – specifically, weight gains are, for all practical purposes, proportional to $\sqrt{t}$ after 1 h to 2 h at 1100 °C. The transient stage comprises rapid variations of the oxidation rate, and was not considered here.

Combining Eqs. (6) and (8), the outgoing Al flux is given by:

$$J_{\mathrm{Al}}^{\mathrm{out}} = \frac{2k_p}{V_{\mathrm{ox}}}\left(2k_p t + X_0^2\right)^{-1/2} \tag{9}$$

The quantity used as a boundary condition in DICTRA is the product $J_{\mathrm{Al}}^{\mathrm{out}} V_{\mathrm{a}}$, where V_{a} is the molar volume of the alloy. The other element fluxes were set to zero. As a consequence, the total amount of matter in the simulation decreased with time. A built-in grid adjustment procedure reduced the node spacing and deleted nodes as needed.

In the presence of a molten silicate, the dissolution of the Al_2O_3 scale modifies the scale growth kinetics. The applicable rate law is discussed in the Appendix. The values of the parameters used in the simulations are given in Table 2.

Table 2 : Parameters used in the simulations.

T (°C)	1100	
t (h)	50	
V_{ox} (cm³/mol)[1]	26.3	
X_0 (nm)	5	
k_d (cm/s$^{1/2}$) [27]	$3.9 \cdot 10^{-7}$	
	Ni-33Co-35Cr-7Al	Ni-28Co-19Cr-11Al
V_a (cm³/mol)[2]	7.35	7.15
k_p (cm²/s) [27]	$9.0 \cdot 10^{-14}$	$1.2 \cdot 10^{-13}$
k_{od} (cm²/s) (Eq. (A3))	$1.8 \cdot 10^{-14}$	$2.7 \cdot 10^{-14}$

[1]Calculated for Al_2O_3 at 1100 °C using data in Ref. [40]

[2]Calculated for the compositions of interest at 1100 °C using Thermo-Calc with TCNI8

3 Simulation Results

The simulated Al, Cr, Co and Ni concentration profiles are compared with experimental profiles in Figures 1-4. Subsurface depletion (for Al) or enrichment (for Cr, Co and Ni) may be described by the shape of the profiles, and by an amplitude defined as the difference between the mole fractions in the bulk and at the metal/oxide interface: $\Delta x_i = \left| x_i^{\text{bulk}} - x_i^{\text{m/o}} \right|$. The Δx_i are found to be larger in the oxidation-dissolution regime than in the oxidation regime: this reflects the increased Al consumption when the Al_2O_3 scale dissolves as it grows. Incidentally, this offers the opportunity to compare the database responses in several concentration ranges.

For both alloys and both regimes, the simulations done with the TCNI8-MOBNI4 combination significantly underestimate Δx_{Al} (Figure 1). The simulated profiles are also found to be less steep, with Al depletion extending to greater depths, compared to the experimental profiles. On the contrary, the NISTCoNi-NISTCoNi-mob simulations are in good agreement with the experimental results. Combining TCNI8 with NISTCoNi-mob, or NISTCoNi with MOBNI4, shows that the difference mainly comes from the mobility database: Δx_{Al} is significantly underestimated in simulations made with MOBNI4, and in better agreement with experimental data in simulations made with NISTCoNi-mob. With a given mobility database, on the other hand, using one or the other thermodynamic database makes little difference. When associated with NISTCoNi-mob, TCNI8 and CRALDAD produce profiles in slightly better agreement with the experimental results, compared to NISTCoNi.

The same trends are observed with the other components. The simulations done with MOBNI4 underestimate Δx_{Cr} (Figure 2) and Δx_{Co} (Figure 3), and produce profiles that are flatter than those measured experimentally. The simulations done with NISTCoNi-mob also tend to underestimate Δx_{Cr} and Δx_{Co}, but are in better agreement with the experimental results. Again the outcome of the simulation is mostly determined by the mobility database, and the influence of the thermodynamic database is secondary. Relative to the experimental results, TCNI8 and CRALDAD produce a slightly better match than NISTCoNi for Cr, while the reverse is observed for Co.

The case of Ni is slightly more complex, as the shape of the Ni profiles when approaching the surface is not monotonic (Figure 4). Nevertheless, the profiles obtained with MOBNI4 are found to be flatter than the experimental profiles, while those generated with NISTCoNi-mob are in generally good agreement. Again the influence of the thermodynamic database is secondary.

4 Discussion

The amplitude of Al depletion, Δx_{Al}, results from a balance between the outgoing Al flux, described in the simulations by Eq. (6), and the flux that can be sustained within the alloy from the bulk to the surface, Eq. (1). At steady state, the Al flux in the alloy matches the outgoing flux imposed by oxidation. The Al flux in the alloy is comprised of $\widetilde{D}_{\text{Al}j}^{\text{Ni}} \frac{\partial C_j}{\partial z}$ products, with $j = \text{Al}$ (main term) and $j = \text{Co}, \text{Cr}$ (cross-terms); for a given flux, smaller diffusivities are compensated by larger concentration gradients, and vice versa. An underestimated Δx_{Al}, as observed in the simulations done with MOBNI4, therefore suggests that $\widetilde{D}_{\text{AlAl}}^{\text{Ni}}$ is too large. The overestimated diffusivity is also reflected in the shape of the profiles generated with MOBNI4 (smaller slopes, Al depletion extending to greater depths). The fact that the thermodynamic database has little influence on the simulated profiles further suggests that the atomic mobility of Al calculated from the MOBNI4 data is overestimated.

The surface enrichment of Cr, Co and Ni is caused by the Al removal to form Al_2O_3. For a given Al loss, the compensating enrichment is split between the three species; it follows that the Cr, Co and Ni concentration gradients are smaller than that of Al. As a consequence, the Al gradient is a relatively important driving force for the Cr, Co and Ni fluxes (via the cross-terms $\widetilde{D}_{k\mathrm{Al}}^{\mathrm{Ni}}$). The relative roles of the cross- and main-terms are not easily identified, and it is difficult to evaluate how appropriate each term of the calculated diffusivity matrix is, based on a small number of profiles. The choice of the thermodynamic database had little impact, and differences between simulations mostly stemmed from the mobility terms. The small differences arising from the choice of the thermodynamic database were not investigated. Instead, the discussion will focus on mobility and compare tracer diffusion coefficients computed with the MOBNI4 and NISTCoNi-mob databases.

Figure 5 shows tracer diffusion coefficients in the fcc solid solution calculated at four compositions: for each alloy, the nominal composition and the composition measured at the metal/oxide interface after reaction in the oxidation-dissolution regime were chosen, so as to cover a wide range of observed conditions. As expected, D_{Al}^{*} is significantly larger when computed from MOBNI4 than from NISTCoNi-mob: the ratio is about 10 in Ni-33Co-35Cr-7Al, and about 3 in Ni-28Co-19Cr-11Al. Values of D_{Ni}^{*} follow the same trend; D_{Cr}^{*} is slightly larger when computed from MOBNI4 (with a ratio between 1 and 2), while for D_{Co}^{*} the ratio is either smaller or larger than one, depending on the composition.

The underlying differences between MOBNI4 and NISTCoNi-mob are readily exposed by examining the composition dependence of the D_i^{*} in binary or pseudo-binary systems, and in particular, by observing the end-member values (not shown here). In particular, such an examination shows that in MOBNI4, D_{Al}^{*} in pure Co, noted $D_{\mathrm{Al}^{*}}^{\mathrm{Co}}$, is equal to $D_{\mathrm{Al}^{*}}^{\mathrm{Ni}}$, i.e., the mobility parameters for Al diffusion in Co were not assessed, and instead were assigned values corresponding to Al diffusion in Ni. In the NISTCoNi-mob database (and in reality), $D_{\mathrm{Al}^{*}}^{\mathrm{Co}}$ is smaller than $D_{\mathrm{Al}^{*}}^{\mathrm{Ni}}$ (about 2.5 times smaller at 1100 °C). As a consequence, MOBNI4 overestimates D_{Al}^{*} in Co-containing alloys, to an extent that increases with the Co content.

Other parameters contribute to the variance between D_{Al}^{*} values computed with MOBNI4 and NISTCoNi. More generally, differences exist between the two databases in the mobility parameters chosen for all combinations of solutes and end-members. A complete discussion of the underlying assessments exceeds the scope of the present paper. Nevertheless, the present work highlights the importance of using critically assessed mobility data relevant for the alloy system of interest, where “alloy system” should be taken in a broad sense. Indeed, the MOBNI4 database was developed for use with Ni-based alloys, and although the mobility description of the binary Co-Ni system is stated to be complete [30], failure to include Al diffusion data for Co-Ni contributes to causing issues when simulating Co-containing alloys. This was particularly apparent here because of the high Co level in the two alloys studied. The NISTCoNi-mob database, on the other hand, includes preliminary assessments for all the Ni- and Co- containing binary (Al-Co, Al-Ni, Co-Cr, Co-Ni, Cr-Ni) and ternary subsystems (Al-Co-Cr, Al-Co-Ni, Al-Cr-Ni, Co-Cr-Ni) of the Al-Co-Cr-Ni system [41]. This proves valuable in describing the diffusion behavior of alloys with high Ni and Co levels.

In the simulations of Ni-33Co-35Cr-7Al in the oxidation-dissolution regime done with NISTCoNi-mob, the Al concentration reaches values close to zero at the metal/oxide interface. Further tests showed that in these conditions, a small increase in the oxidation constant k_p, or a small change in other parameters such as the dissolution constant or

the oxide or alloy molar volume, could cause the simulation to fail, due to the Al concentration reaching zero (at which point the Al flux imposed by oxidation cannot be sustained without entering negative concentrations). This behavior is consistent with the experiments: in molten sodium silicate, Ni-33Co-35Cr-7Al locally failed to sustain Al_2O_3 growth, and formed Cr_2O_3 instead [27]. Using this type of simulations, it is thus possible to estimate whether an alloy will be susceptible to local failure, should there be some metallurgical defect or chemical inhomogeneity at the alloy surface or in the scale (which always occurs in practice). The reliability of the estimation, of course, depends on the input data (oxidation and dissolution constants) as well as the databases.

The need for accurate descriptions of atomic mobility in multicomponent systems is evident from the present work. The development of mobility databases is a continuous process; as new diffusion models and new experimental or theoretical data become available, new assessments and re-assessments are needed, which can constitute a time-limiting factor in materials design. One important aspect in producing mobility assessments more efficiently is that experimental and theoretical diffusion data should be easily accessible and searchable. The main sources for mobility assessments are interdiffusion and tracer diffusion data; one effort to make such data more accessible is the online Phase-Based Data Repository from NIST [42]. This includes a collection of easily comparable measured and calculated, self-diffusion and impurity diffusion coefficients, as well as access to experimental data used to determine interdiffusion coefficients through the NIST Materials Data Curation System [43].

5 Concluding Remarks

The present work showed that the DICTRA module of Thermo-Calc can be applied to simulate subsurface composition profiles arising from selective oxidation in multicomponent systems, provided that appropriate thermodynamic and mobility databases are available. Various service conditions and associated reaction regimes can be simulated by setting component fluxes at the alloy surface as boundary conditions, which requires prior knowledge of the oxidation rate. Here, simple analytical expressions were used to describe the outward Al flux associated with exclusive Al_2O_3 growth in pure oxidation and oxidation-dissolution regimes, based on experimental data. The simulations successfully reproduced composition profiles measured in γ NiCoCrAl alloys; in particular, the detrimental effect of an increased Al consumption due to Al_2O_3 dissolution in a molten silicate was illustrated. This type of simulation can be used to evaluate the minimum Al concentration required for exclusive Al_2O_3 formation, in particular in concentrated alloys where the concentration dependence of the interdiffusion coefficients is significant and cannot be handled with analytical models.

The use of different database combinations highlighted the roles played by the thermodynamic factors and the atomic mobilities in the interdiffusion coefficients, and in turn in the simulated concentration profiles. In the conditions tested (concentrated single-phase γ NiCoCrAl alloys at 1100 °C), the thermodynamic factors obtained from the TCNI8, NISTCoNi and CRALDAD databases were all similar, and the differences between the simulations mostly stemmed from the description of atomic mobility, i.e., from the diffusion mobility databases. Specifically, the profiles obtained with NISTCoNi-mob were in good agreement with the available experimental results, while those obtained with MOBNI4 were not. This was due, in part, to an inadequate description of Al diffusion in Co in MOBNI4.

Acknowledgements

This work stemmed from earlier work carried out by the authors while at the University of Pittsburgh (TG) and at NIST (GL). Our fruitful collaborations with Brian Gleeson in Pittsburgh and with Carelyn Campbell and the Thermodynamics and Kinetics Group at NIST are acknowledged.

References

[1] C. Wagner, *Journal of the Electrochemical Society* **99** (1952) 369–380
[2] F. Gesmundo, F. Viani, Y. Niu and D.L. Douglass, *Oxidation of Metals* **40** (1993) 373-393
[3] F. Gesmundo, F. Viani, Y. Niu and D.L. Douglass, *Oxidation of Metals* **42** (1994) 465–483
[4] F. Gesmundo, P. Castello, F. Viani and J. Philibert, *Oxidation of Metals* **47** (1997) 91–115
[5] F. Gesmundo, P. Castello, F. Viani and J. Philibert, *Oxidation of Metals* **47** (1997) 525–550
[6] Y. Niu and F. Gesmundo, *Oxidation of Metals* **56** (2001) 517-536
[7] J.A. Nesbitt, *Oxidation of Metals* **44** (1995) 309–338
[8] D.P. Whittle, D.J. Evans, D.B. Scully and G.C. Wood, *Acta Metallurgica* **15** (1967) 1421–1430
[9] J.A. Nesbitt and R.W. Heckel, *Thin Solid Films* **119** (1984) 281–290
[10] J.A. Nesbitt, *Journal of the Electrochemical Society* **136** (1989) 1518–1527
[11] E.Y. Lee, D.M. Chartier, R.R. Biederman and R.D. Sisson, *Surface and Coatings Technology* **32** (1987) 19–39
[12] N. Saunders and A.P. Miodownik, CALPHAD (Calculation of Phase Diagrams): A Comprehensive Guide, Pergamon, 1998
[13] H.L. Lukas, S.G. Fries and Bo Sundman, Computational Thermodynamics: The Calphad Method, Cambridge University Press, 2007
[14] A. Borgenstam, L. Höglund, J. Ågren and A. Engström, *Journal of Phase Equilibria* **21** (2000) 269-280
[15] B. Sundman, U.R. Kattner, C. Sigli, M. Stratmann, R. Le Tellier, M. Palumbo and S.G. Fries, *Computational Materials Science* **125** (2016) 188–196
[16] J.-O. Andersson, T. Helander, L. Höglund, P. Shi and B. Sundman, *Calphad* **26** (2002) 273-312
[17] Thermo-Calc Software Ni-based Superalloys Database
[18] Thermo-Calc Software Ni-alloys Mobility Database
[19] R.H. Davies, A.T. Dinsdale, J.A. Gisby, J.A.J. Robinson and S.M. Martin, *Calphad* **26** (2002) 229-271
[20] ThermoTech Ni-based Superalloys Database
[21] T.J. Nijdam and W.G. Sloof, *Acta Materialia* **56** (2008) 4972–4983
[22] M.S.A. Karunaratne, S.L. Ogden, S.D. Kenny and R.C. Thomson, *Materials Science and Technology* **25** (2009) 287–299
[23] M. Bensch, A. Sato, N. Warnken, E. Affeldt, R.C. Reed and U. Glatzel, *Acta Materialia* **60** (2012) 5468–5480
[24] R. Pillai, W.G. Sloof, A. Chyrkin, L. Singheiser and W.J. Quadakkers, *Materials at High Temperatures* **32** (2015) 57–67
[25] K. Yuan, R. Eriksson, R. Lin Peng, X.-H. Li, S. Johansson and Y.-D. Wang, *Surface and*

Coatings Technology **232** (2013) 204–215
[26] H. Chen and T. Barman, *Computational Materials Science* **147** (2018) 103-114
[27] T. Gheno and B. Gleeson, *Oxidation of Metals* **87** (2017) 527-539
[28] J.O. Andersson and J. Ågren, *Journal of Applied Physics* **72** (1992) 1350-1355
[29] http://www.thermocalc.com/media/23650/tcni8_extended_info.pdf, accessed July 13, 2018
[30] http://www.thermocalc.com/media/23657/mobni4.pdf, accessed July 13, 2018
[31] http://chimad.northwestern.edu/, accessed July 13, 2018
[32] U.R. Kattner, Construction of a thermodynamic database for Ni-base superalloys: A case study, in P.E.A. Turchi, A. Gonis, R.D. Shull (eds.), CALPHAD and alloy thermodynamics, TMS, Warrendale (USA), 2002, pp. 147-164
[33] C.E. Campbell, W.J. Boettinger and U.R. Kattner, *Acta Materialia* **50** (2002) 775-792
[34] A. Suzuki, H. Inui and T.M. Pollock, *Annual Review of Materials Research* **45** (2015) 345-368
[35] T. Gheno, X.L. Liu, G. Lindwall, Z.-K. Liu and B. Gleeson, *Science and Technology of Advanced Materials* **16** (2015) 055001
[36] X.L. Liu, G. Lindwall, T. Gheno and Z.-K. Liu, *Calphad* **52** (2016) 125–142
[37] H. Larsson and L. Höglund, *Calphad* **33** (2009) 495–501
[38] T. Gheno and B. Gleeson, *Oxidation of Metals* **86** (2016) 385-406
[39] T. Gheno, G.H. Meier and B. Gleeson, *Oxidation of Metals* **84** (2015) 185-209
[40] G. Fiquet, P. Richet and G. Montagnac, *Physics and Chemistry of Minerals* **27** (1999) 103-111
[41] G. Lindwall, K.-W. Moon, E. Lass, P. Wang, U.R. Kattner and C.E. Campbell, Multicomponent Diffusion Mobility Descriptions for Co Based Superalloys, Materials Science & Technology Technical Meeting and Exhibition, Pittsburgh, 2017
[42] https://phasedata.nist.gov/, accessed July 16, 2018
[43] A. Dima, S. Bhaskarla, C. Becker et al., *JOM* **68** (2016) 2053–2064
[44] E. Jones, E. Oliphant, P. Peterson et al., SciPy: Open Source Scientific Tools for Python, 2001-, http://www.scipy.org/, accessed June 1, 2018

Appendix: modeling oxidation-dissolution kinetics

In the presence of a molten sodium silicate (NS), the Al_2O_3 scale grows by oxidation of the alloy and dissolves in the liquid simultaneously. The net scale growth rate is obtained by adding the production rate, given by Eq. (7), and the dissolution rate. Assuming a constant Al diffusivity in NS and an infinite volume of NS, and neglecting convection, one obtains [27]:

$$\frac{\mathrm{d}X}{\mathrm{d}t} = \frac{k_p}{X} - \frac{k_d}{\sqrt{t}} \tag{A1}$$

where k_d is the dissolution constant, defined as:

$$k_d = \frac{1}{2}\frac{V_{\mathrm{ox}}}{V_{\mathrm{NS}}} N_{\mathrm{Al}}^{\mathrm{o/s}} \sqrt{\frac{D_{\mathrm{Al}}^{\mathrm{NS}}}{\pi}} \tag{A2}$$

with V_{NS} the molar volume of NS, and $N_{\mathrm{Al}}^{\mathrm{o/s}}$ and $D_{\mathrm{Al}}^{\mathrm{NS}}$ the solubility and diffusion coefficient of Al in NS, respectively.

Figure A1 shows the scale growth kinetics obtained by numerical integration of Eq. (A1) for different values of the initial thickness X_0 (using the odeint function of the scipy.integrate Python package [44]). Relatively large values of X_0 have been used for

illustration purposes. At first, the thickness decreases as oxidation (the k_p/X term) is relatively slow due to the pre-existing scale, and dissolution (the $k_d/\sqrt{t}$ term) predominates. This causes oxidation to accelerate, until its rate equals that of dissolution and a minimum thickness is reached. As the Al_2O_3 concentration in the NS increases, dissolution slows down and oxidation becomes predominant: the scale thickens. The tipping point occurs at later times for larger values of X_0. However, the thickness eventually follows a time evolution that is practically independent of X_0. The asymptote is obtained as the solution to Eq. (A1) for $X_0 = 0$, and has a simple analytical form [27]:

$$X^2 = 2k_{od}t$$
$$k_{od} = k_d^2 + k_p - k_d\sqrt{k_d^2 + 2k_p} \quad \text{(A3)}$$

The simulations of oxidation in air were done with an initial thickness that would correspond to a native scale, $X_0 = 5$ nm. With such a small X_0 value, Eq. (A3) is a good approximation of oxidation-dissolution kinetics. It was therefore used in the simulations.

Equation (A1) is based on the hypothesis that in the oxidation-dissolution regime, oxidation proceeds at a rate inversely proportional to the scale thickness, with the same proportionality constant (k_p) as in the oxidation regime, i.e., with the same scale diffusion properties and boundary defect concentrations. In this hypothesis, the outgoing Al flux is still given by Eq. (6), only now with X given by Eq. (A3). This yields:

$$J_{\mathrm{Al}}^{\mathrm{out}} = \frac{2k_p}{V_{\mathrm{ox}}}(2k_{od}t)^{-1/2} \quad \text{(A4)}$$

Figure Captions

Figure 1 : Al concentration profiles in the oxidation and oxidation-dissolution regimes simulated using DICTRA with the parameters in Table 2 and the indicated databases. Experimental profiles obtained by electron-probe microanalysis (EPMA) after reaction in air and in molten sodium silicate, 50 h at 1100 °C [27].

Figure 2 : Cr concentration profiles in the oxidation and oxidation-dissolution regimes simulated using DICTRA with the parameters in Table 2 and the indicated databases. Experimental data: EPMA [27].

Figure 3 : Co concentration profiles in the oxidation and oxidation-dissolution regimes simulated using DICTRA with the parameters in Table 2 and the indicated databases. Experimental data: EPMA [27].

Figure 4 : Ni concentration profiles in the oxidation and oxidation-dissolution regimes simulated using DICTRA with the parameters in Table 2 and the indicated databases. Experimental data: EPMA [27].

Figure 5 : Comparison of tracer diffusivities calculated using the MOBNI4 and NISTCoNi-mob databases at 1100 °C, at the indicated compositions.

Figure A1: Scale growth kinetics in the oxidation and oxidation-dissolution regimes (numerical integration of Eq. (A1) and asymptotic solution for $X_0 = 0$). Large X_0 values were used for illustration purposes. All other parameters are from Table 2.

Figure 1

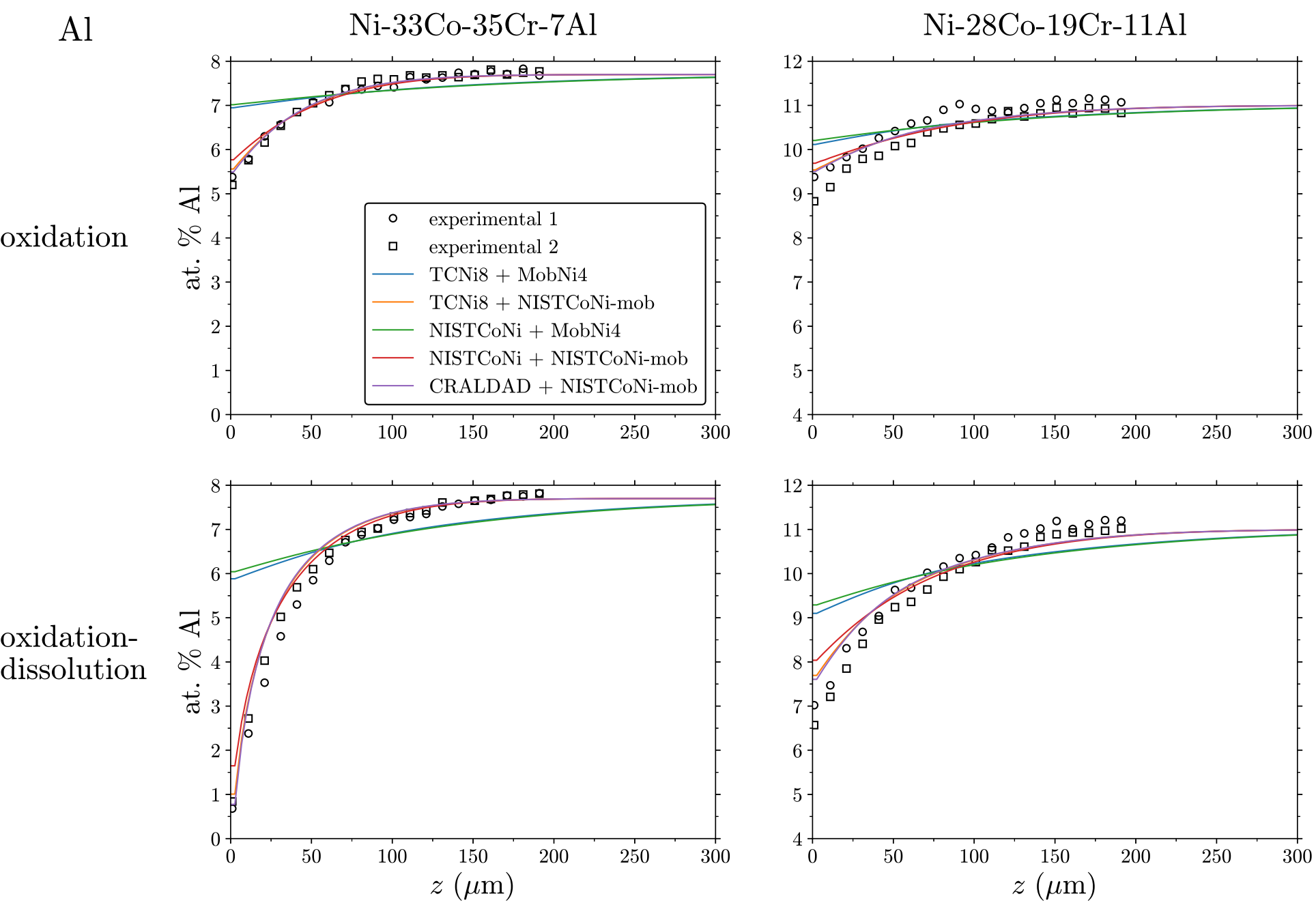
Al
Ni-33Co-35Cr-7Al
Ni-28Co-19Cr-11Al
oxidation
oxidation-dissolution
at. % Al
z (μm)
experimental 1
experimental 2
TCNi8 + MobNi4
TCNi8 + NISTCoNi-mob
NISTCoNi + MobNi4
NISTCoNi + NISTCoNi-mob
CRALDAD + NISTCoNi-mob

Figure 2

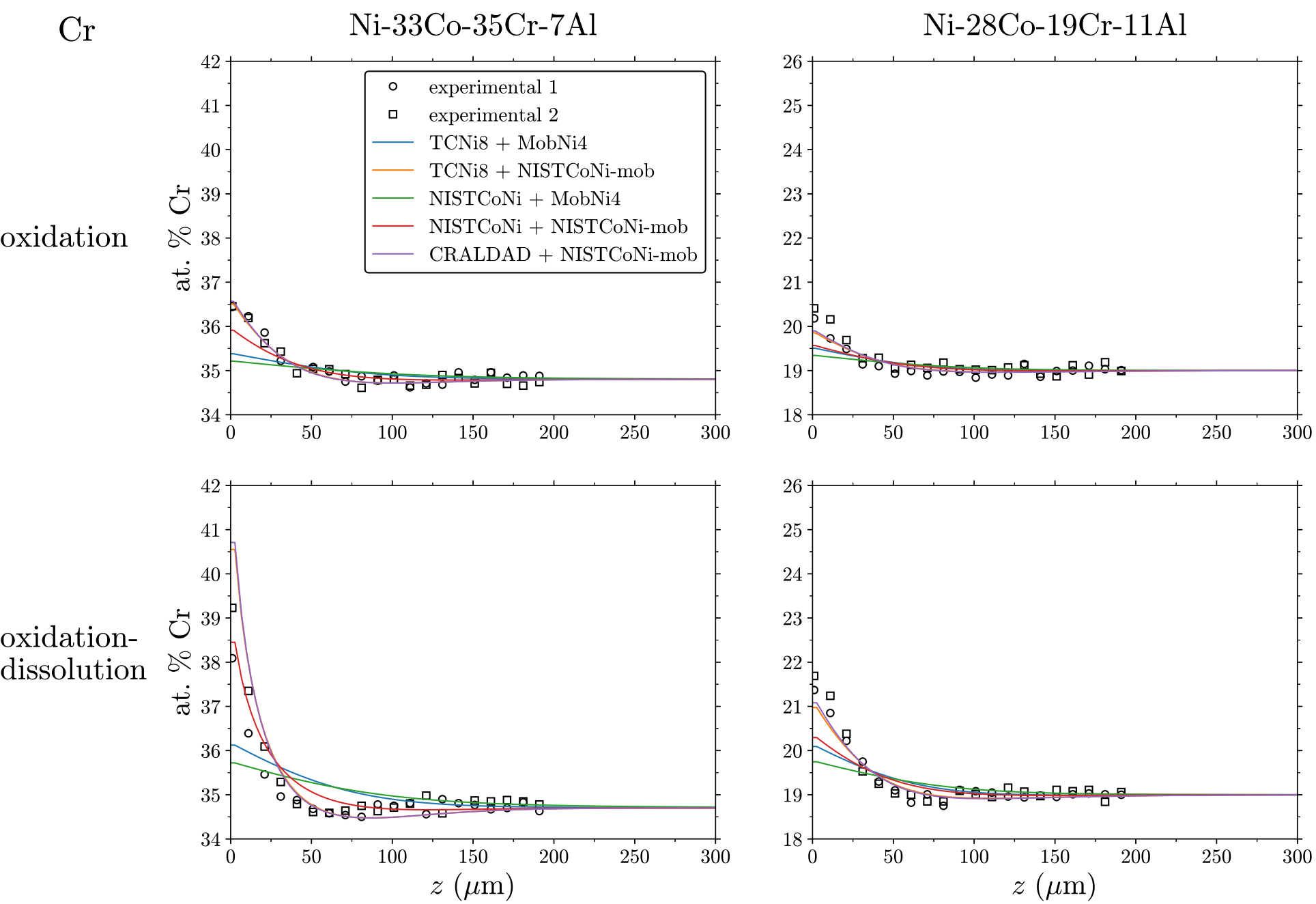
Cr
Ni-33Co-35Cr-7Al
Ni-28Co-19Cr-11Al
oxidation
oxidation-dissolution
at. % Cr
z (μm)
experimental 1
experimental 2
TCNi8 + MobNi4
TCNi8 + NISTCoNi-mob
NISTCoNi + MobNi4
NISTCoNi + NISTCoNi-mob
CRALDAD + NISTCoNi-mob

Figure 3

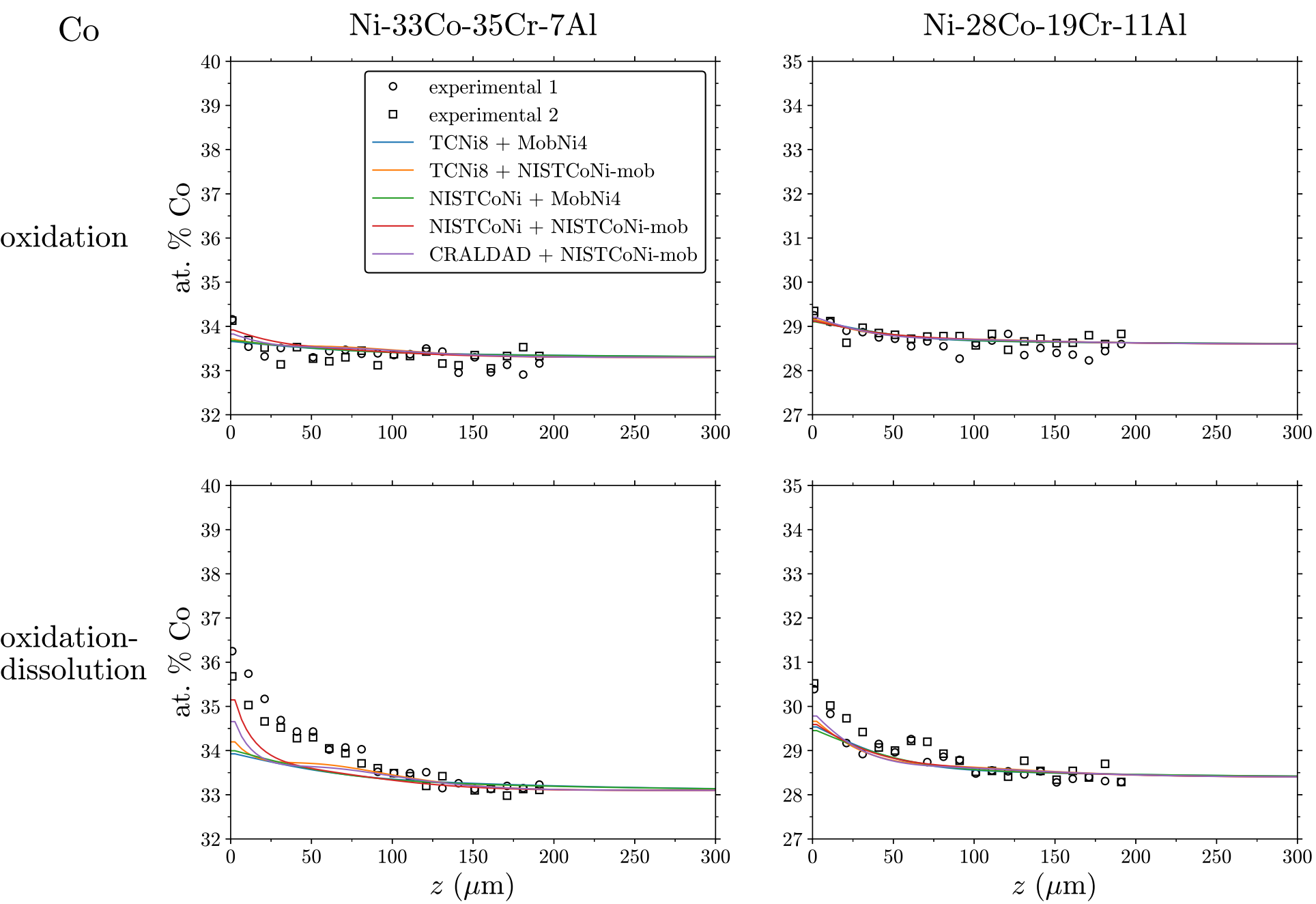
Co
Ni-33Co-35Cr-7Al
Ni-28Co-19Cr-11Al
oxidation
oxidation-dissolution
at. % Co
z (μm)
experimental 1
experimental 2
TCNi8 + MobNi4
TCNi8 + NISTCoNi-mob
NISTCoNi + MobNi4
NISTCoNi + NISTCoNi-mob
CRALDAD + NISTCoNi-mob

Figure 4

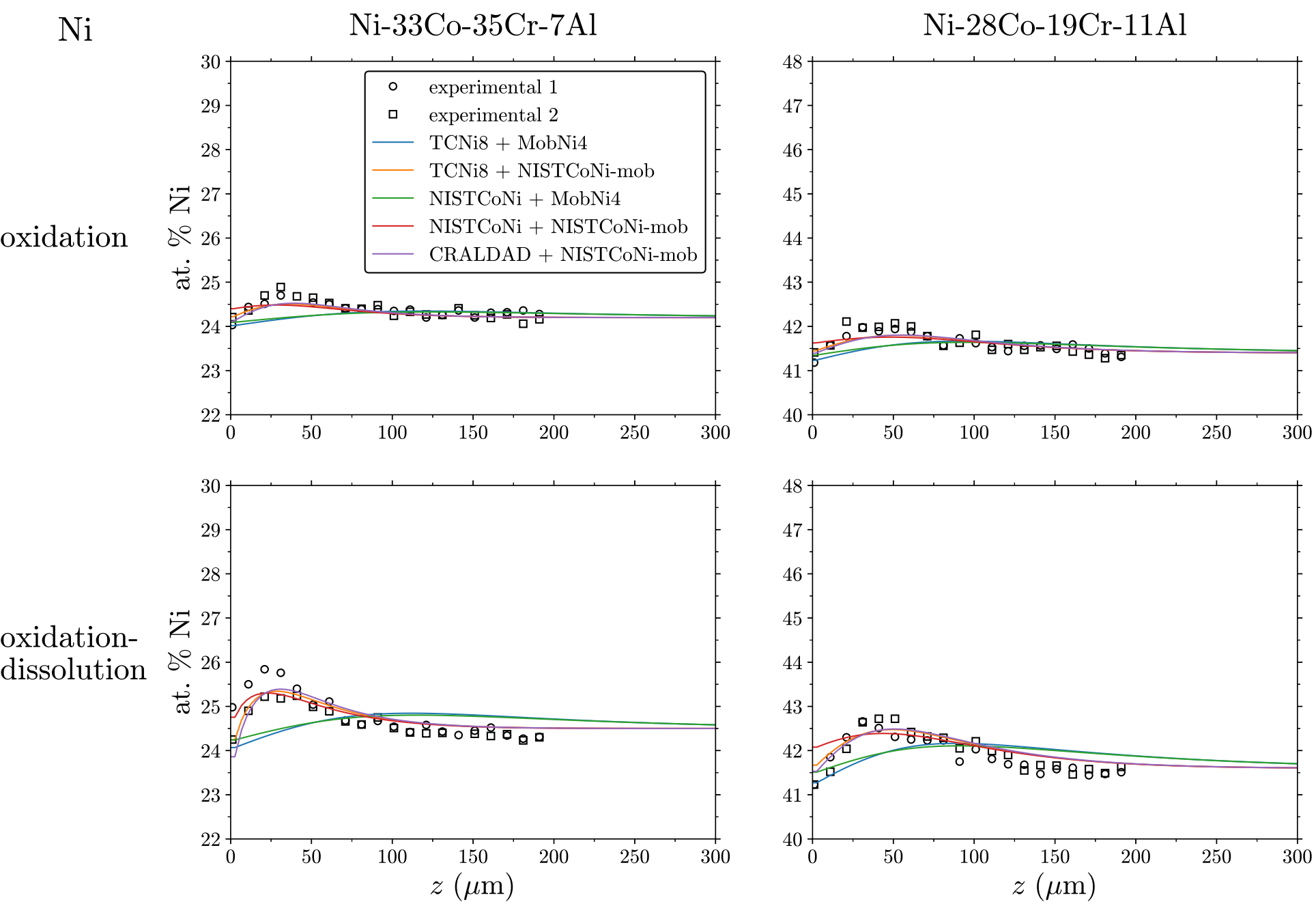
Ni
Ni-33Co-35Cr-7Al
Ni-28Co-19Cr-11Al
oxidation
oxidation-dissolution
at. % Ni
z (μm)
experimental 1
experimental 2
TCNi8 + MobNi4
TCNi8 + NISTCoNi-mob
NISTCoNi + MobNi4
NISTCoNi + NISTCoNi-mob
CRALDAD + NISTCoNi-mob

Figure 5

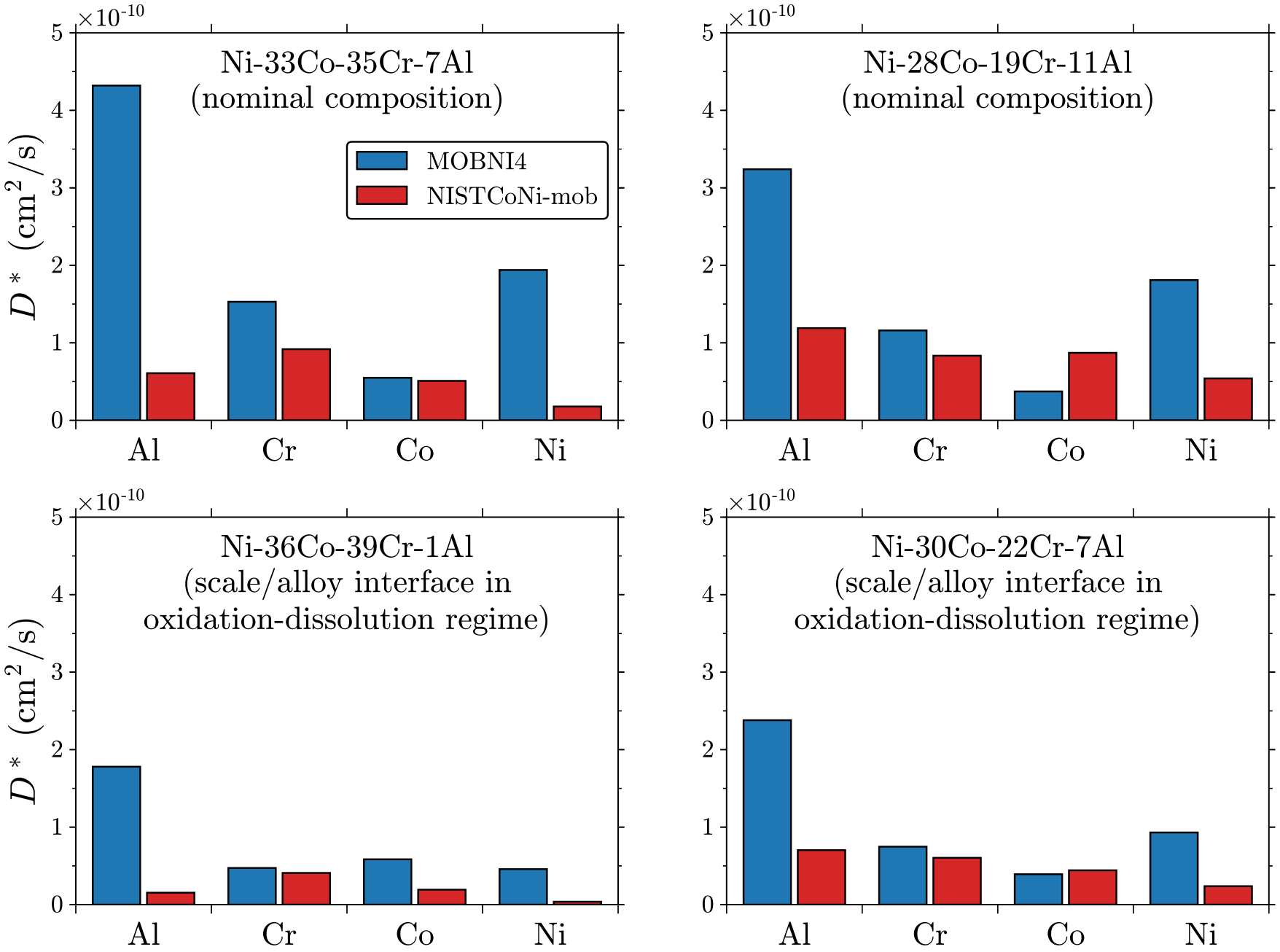
×10-10
Ni-33Co-35Cr-7Al
(nominal composition)
MOBNI4
NISTCoNi-mob
D* (cm2/s)
Al
Cr
Co
Ni
Ni-28Co-19Cr-11Al
(nominal composition)
Ni-36Co-39Cr-1Al
(scale/alloy interface in
oxidation-dissolution regime)
Ni-30Co-22Cr-7Al
(scale/alloy interface in
oxidation-dissolution regime)

Figure A1

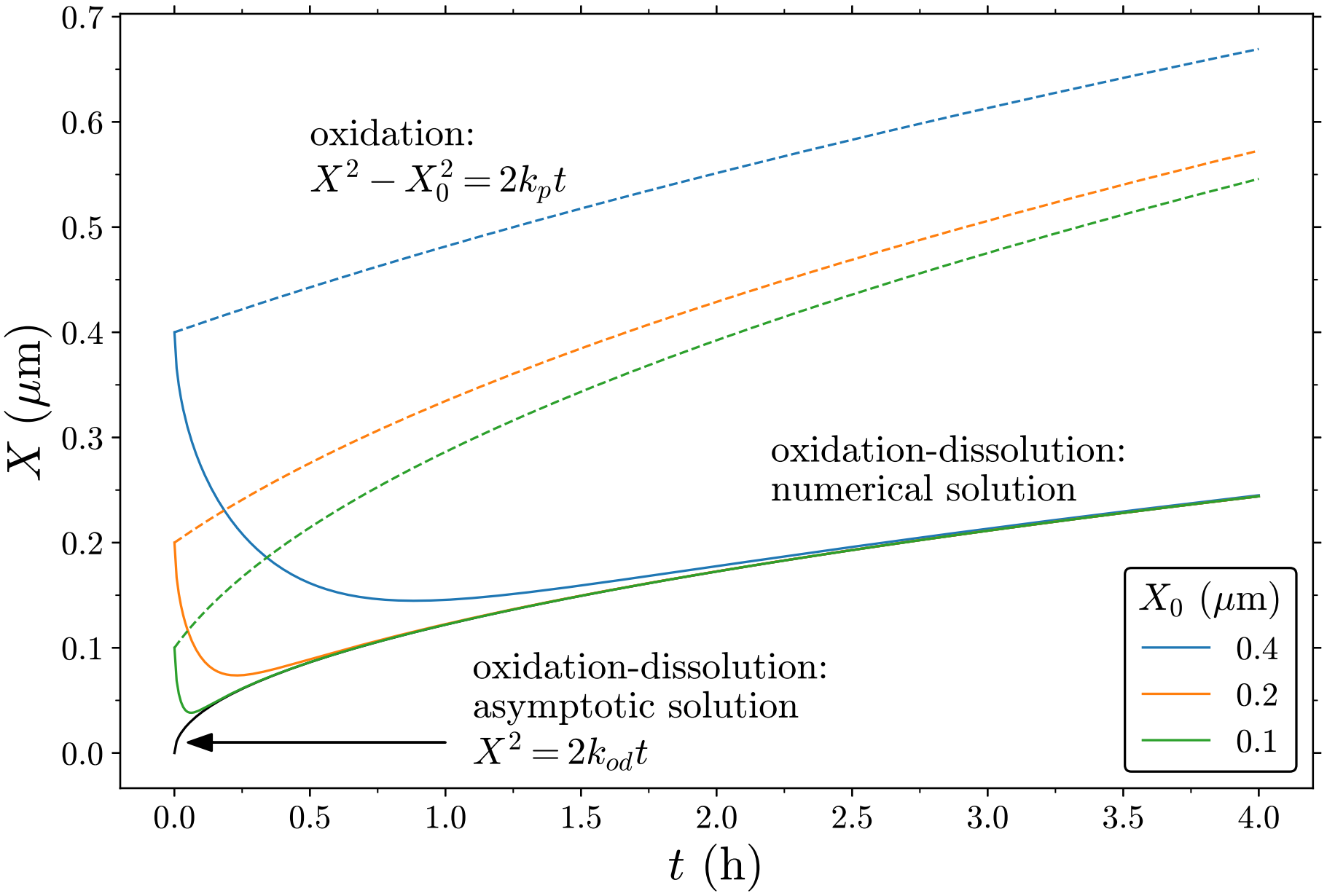

This is a post-peer-review, pre-copyedit version of an article published in Oxidation of Metals. The final authenticated version is available online at: http://dx.doi.org/10.1007/s11085-018-9877-y"